Algorithm Theoretical Basis Document for Vantor ACOMP Surface Reflectance Product

Release date: April 6, 2026

Contact:

Michele Kuester, PhD.
michele.kuester@maxar.com

Tina Ochoa
tina.ochoa@maxar.com

Document Version History

Version	Date	Author	Change Description
A	04/06/2026	Michele Kuester	Pre-release draft
B	04/09/2026	Michele Kuester, Tina Ochoa	Reviewed for science

Please submit any comments or updates to michele.kuester@vantor.com or tina.ochoa@vantor.com

Table of Contents

List of Tables

List of Figures

1 Introduction

1.1 Overview

ACOMP is a radiative transfer–based atmospheric correction algorithm that converts top-of-atmosphere (TOA) radiance into surface reflectance using precomputed lookup tables (LUTs) derived from radiative transfer modeling of atmospheric scattering and absorption. The algorithm enables radiometrically consistent analysis across sensors, acquisition times, and geographic regions.

This document describes the theoretical basis and implementation of the ACOMP Surface Reflectance algorithm. It outlines the scientific framework, assumptions, and computational methods used to correct TOA radiance for atmospheric effects, including molecular (Rayleigh) scattering, aerosol scattering, and gaseous absorption, in order to retrieve surface reflectance. The ATBD serves as a reference for product users and validation teams, supporting interpretation, application, and evaluation of the ACOMP surface reflectance product.

1.2 Scope

This Algorithm Theoretical Basis Document (ATBD) defines the scientific foundation, assumptions, and implementation details of the ACOMP surface reflectance algorithm. It describes the radiative transfer framework, atmospheric correction methodology, and computational approach used to derive surface reflectance from satellite observations.

The document specifies required input data, generated outputs, and processing workflows, and characterizes sources of uncertainty and expected performance. It also provides guidance for product interpretation and use, including limitations and considerations relevant to scientific and operational applications.

1.3 Acronyms, Abbreviations, Terms

Table 1. Acronyms

Acronym	Definition
ACOMP	Atmospheric Compensation
AERONET	AErosol RObotic NETwork
AOD	Aerosol Optical Depth
ASD	Analytical Spectral Devices (field spectrometer)

Acronym	Definition
ATBD	Algorithm Theoretical Basis Document
BRDF	Bidirectional Reflectance Distribution Function
DEM	Digital Elevation Model
DN	Digital Number
DOS	Dark Object Subtraction
FLAASH	Fast Line-of-sight Atmospheric Analysis of Spectral Hypercubes
H_2O	Water Vapor
LUT	Lookup Table
MIO	Mid-Inclination Orbit
MODIS	Moderate Resolution Imaging Spectroradiometer
MODTRAN	MODerate resolution atmospheric TRANsmission (radiative transfer model)
NDVI	Normalized Difference Vegetation Index
O_2	Molecular Oxygen
O_3	Ozone
QUAC	Quick Atmospheric Correction
RMSE	Root Mean Square Error
SWIR	Shortwave Infrared
TOA	Top Of Atmosphere
VNIR	Visible and Near Infrared

The following symbols are used throughout this document to describe radiative transfer processes, atmospheric parameters, and surface reflectance retrieval.

Table 2. Symbols and Notation

Symbol	Definition	Units
ρ	Surface reflectance	unitless
ρ_s	Retrieved surface reflectance	unitless

Symbol	Definition	Units
ρ_{scaled}	Scaled surface reflectance value	integer
L	Radiance (generic)	$W \cdot m^{-2} \cdot sr^{-1} \cdot \mu m^{-1}$
L_{TOA}	Top-of-atmosphere radiance	$W \cdot m^{-2} \cdot sr^{-1} \cdot \mu m^{-1}$
L_p	Atmospheric path radiance	$W \cdot m^{-2} \cdot sr^{-1} \cdot \mu m^{-1}$
L_{adj}	Adjacency radiance contribution	$W \cdot m^{-2} \cdot sr^{-1} \cdot \mu m^{-1}$
E_0	Extraterrestrial solar irradiance	$W \cdot m^{-2} \cdot \mu m^{-1}$
T_d	Downward atmospheric transmittance	unitless
T_u	Upward atmospheric transmittance	unitless
T	Total atmospheric transmittance	unitless
θ_s	Solar zenith angle	degrees
θ_v	Sensor (view) zenith angle	degrees
ϕ	Relative azimuth angle	degrees
τ	Optical depth (generic)	unitless
τ_a	Aerosol optical depth (AOD)	unitless
τ_R	Rayleigh (molecular) optical depth	unitless
λ	Wavelength	μm
r	Particle radius (aerosols)	μm
P	Atmospheric pressure	Pa
P_0	Standard atmospheric pressure	Pa
z	Surface elevation	m
g	Gravitational acceleration	$m \cdot s^{-2}$
R	Specific gas constant for dry air	$J \cdot kg^{-1} \cdot K^{-1}$
T	Atmospheric temperature	K
$k(\lambda)$	Absorption coefficient at wavelength λ	$m^2 \cdot kg^{-1}$ (or equivalent)
u	Column gas abundance	$kg \cdot m^{-2}$ (or atm-cm depending on convention)

Symbol	Definition	Units
S	Reflectance scaling factor	unitless
DN	Digital number (pixel value)	integer
σ_x	Uncertainty in variable x	variable-dependent
$\Delta\rho$	Change in reflectance due to perturbation	unitless
$f(\cdot)$	Functional relationship in retrieval model	—
w_i	Weighting coefficient (e.g., interpolation, kriging)	unitless
$K(x_i, x_j)$	Spatial covariance/kernel function	unitless

2. Background

Satellite sensors measure radiance at the top of the atmosphere (TOA), which includes contributions from both the Earth's surface and the atmosphere. As solar radiation propagates through the atmosphere, it is modified by molecular (Rayleigh) scattering, aerosol scattering, and absorption by atmospheric gases such as water vapor, ozone, and oxygen. These processes alter both the magnitude and spectral characteristics of the observed signal, introducing variability that depends on atmospheric conditions, viewing geometry, and wavelength. As a result, TOA measurements alone are not directly comparable across time, location, or sensor.

Surface reflectance represents the intrinsic optical properties of surface materials and is defined as the ratio of reflected radiance to incident solar irradiance under specified illumination and viewing conditions. By removing atmospheric effects, surface reflectance provides a physically meaningful and consistent quantity that enables quantitative analysis across acquisitions. This consistency is essential for applications such as vegetation monitoring, land cover classification, environmental change detection, agricultural assessment, and multi-temporal analysis.

The Atmospheric Compensation (ACOMP) algorithm addresses these challenges by converting TOA radiance into surface reflectance using a physics-based atmospheric correction framework. The algorithm represents atmospheric processes through radiative transfer theory, accounting for scattering and absorption effects in a consistent manner. Rather than solving the full radiative transfer equations explicitly for each pixel, ACOMP leverages precomputed radiative transfer simulations implemented as lookup tables (LUTs), enabling efficient and scalable processing.

Within this framework, atmospheric parameters such as aerosol optical depth and water vapor are estimated using a combination of scene-based retrieval methods and ancillary data. These

parameters are used to interpolate within the LUTs to derive atmospheric correction terms, including path radiance and transmittance, which are then used to retrieve surface reflectance.

ACOMP is designed as an automated atmospheric correction framework capable of processing large volumes of high-resolution imagery without manual intervention. By combining physics-based modeling, LUT-based implementation, and scene-dependent parameter estimation, the algorithm produces consistent and repeatable surface reflectance products across diverse atmospheric conditions, geographic regions, and sensor platforms.

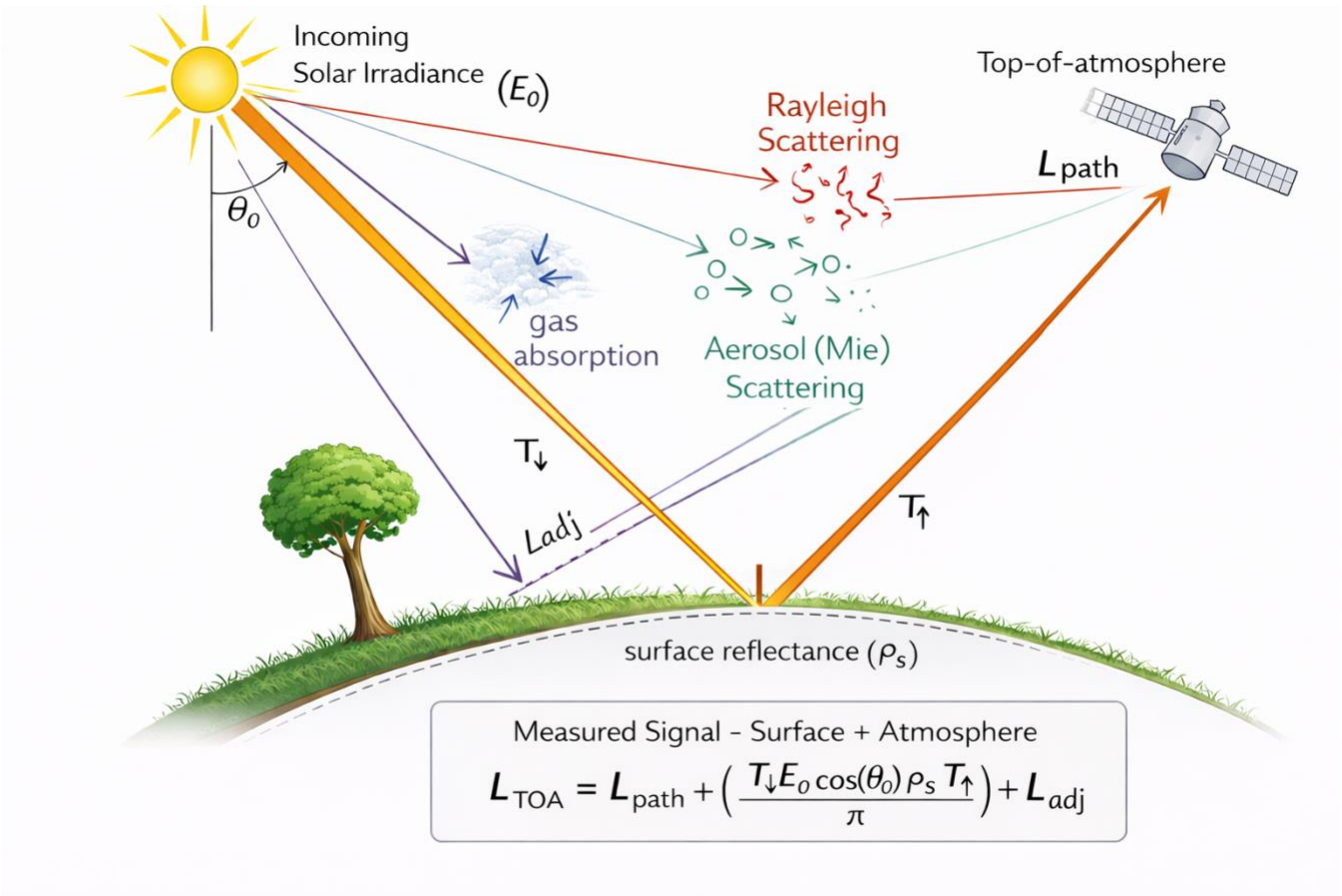

Figure 1. Conceptual diagram of atmospheric correction illustrating the inclusion of atmospheric scattering and absorption effects, as well as adjacency effects, to retrieve surface reflectance from top-of-atmosphere radiance measurements

3. Product Description

3.1 Product Overview

The ACOMP (Atmospheric Compensation) algorithm generates surface reflectance products from optical satellite imagery by correcting top-of-atmosphere (TOA) radiance measurements for the effects of atmospheric scattering and absorption. TOA radiance observed by satellite sensors includes contributions from the Earth's surface as well as interactions with atmospheric molecules, aerosols, and absorbing gases. ACOMP applies a physics-informed and LUT driven atmospheric correction framework to estimate atmospheric parameters and remove these effects, accounting for molecular (Rayleigh) scattering, aerosol scattering, and gaseous absorption.

The resulting surface reflectance product represents the intrinsic spectral properties of surface materials under standardized illumination and viewing conditions. By removing atmospheric variability, the product enables consistent and physically meaningful comparison of observations across different acquisition dates, geographic regions, and atmospheric states.

ACOMP-derived surface reflectance supports a wide range of scientific and operational applications, including land cover classification, vegetation monitoring, environmental change detection, agricultural assessment, coastal and inland water analysis, and multi-temporal studies of high-resolution imagery. By providing atmospherically normalized reflectance measurements, the product enables quantitative remote sensing analysis and supports integration of satellite data into scientific models and decision-support systems.

3.2 Input Data

The ACOMP algorithm requires as primary input a calibrated image and its corresponding metadata file. The input imagery consists of pixel digital numbers (DNs), which are converted to top-of-atmosphere (TOA) radiance using sensor-specific calibration parameters provided in the metadata. The metadata additionally supplies acquisition geometry, including solar and sensor viewing angles, acquisition time, and geolocation, all of which define the radiative transfer conditions for the scene.

In addition to image and metadata inputs, ACOMP utilizes ancillary environmental datasets to characterize atmospheric and surface conditions. These include surface elevation, atmospheric state parameters, and climatological estimates of aerosol optical depth and water vapor. For certain processing configurations, externally derived aerosol optical depth (AOD) maps may also be provided to guide the retrieval.

Surface elevation is obtained from a digital elevation model (DEM) contained within the ACOMP processing database. The geographic extent of the input scene is determined from image metadata, and the corresponding DEM region is sampled. A representative mean elevation is computed over the scene footprint and used as an input to the radiative transfer modeling. This parameter influences atmospheric pressure, optical path length, and scattering behavior. The current implementation assumes spatially uniform elevation across the scene, which is generally appropriate for moderate terrain variability but may introduce uncertainty in areas of significant topographic relief.

Atmospheric properties are initialized using climatological datasets included in the ACOMP database. These datasets provide location- and season-dependent estimates of atmospheric profiles, aerosol loading, and water vapor. Within the ACOMP framework, these values serve as initial conditions for the atmospheric correction.

Aerosol properties are subsequently refined using a scene-based atmospheric retrieval approach, in which atmospheric parameters are estimated directly from the observed imagery in a manner consistent with radiative transfer physics. Specifically, ACOMP evaluates candidate aerosol optical depth values by comparing observed TOA radiance with radiative transfer simulations represented in precomputed lookup tables. The AOD that best reconciles modeled and observed radiance is selected as the optimal solution. This retrieval may be performed globally or at the pixel level to capture spatial variability in atmospheric conditions. When image-based constraints are insufficient, the algorithm reverts to climatological estimates to ensure stable performance.

Table 3. A summary of the primary input data required by the algorithm.

Input	Source	Description
Pixel Digital Numbers (DN)	Level-1 sensor imagery	Raw detector counts representing measured radiance at the sensor aperture
Radiometric Calibration Parameters	Sensor metadata / calibration files	Gain and offset values used to convert DN to TOA radiance
Solar Geometry	Sensor metadata	Solar zenith and azimuth angles at acquisition time
Viewing Geometry	Sensor metadata	Sensor viewing angles (zenith and azimuth) defining observation geometry
Acquisition Time	Sensor metadata	Date and time of acquisition used for Earth–Sun distance and atmospheric state selection
Spectral Response Functions	Sensor database	Band-specific spectral response used in radiative transfer calculations and LUT generation

Input	Source	Description
Atmospheric Profiles	Climatological database	Temperature and pressure profiles used to define the atmospheric model (e.g., tropical, mid-latitude)
Water Vapor	Climatology and/or scene-based retrieval	Initial estimate from ancillary data, optionally refined from image-based retrieval (sensor-dependent)
Aerosol Optical Depth (AOD)	Scene-based retrieval and/or climatology	Estimated by matching observed radiance to LUT-based radiative transfer simulations; fallback to climatology when needed
Aerosol Model Type	Climatological database	Aerosol type (e.g., rural, maritime, urban, desert) selected based on land cover and proximity to water
Surface Elevation	DEM (ACOMP database)	Mean scene elevation used to adjust atmospheric pressure and optical path length
Land Cover Classification	Global land cover dataset	Used to inform aerosol model selection and atmospheric initialization
External AOD Map (optional)	User-provided or prior processing	Precomputed AOD used to guide retrieval when spectral information is limited (e.g., non-VNIR bands)
Processing Configuration Parameters	User-defined inputs	Controls algorithm behavior (e.g., LUT vs. MODTRAN, AOD mode, output format, bit depth, auxiliary outputs)

3.3 Output Data

The primary output of the ACOMP algorithm is a surface reflectance image representing the estimated reflectance at the Earth's surface after removal of atmospheric effects. Surface reflectance is produced for each spectral band of the input sensor and corresponds to the reflectance that would be observed under idealized, atmosphere-free conditions.

Surface reflectance values may be stored either as floating-point values in the range $[0, 1]$or as scaled integers, depending on the selected output configuration. In the case of scaled integer products, reflectance is represented as:

$$\rho_{scaled} = \rho_s \times S$$

where $\rho_s$is surface reflectance and $S$is a scale factor determined by the data delivery pathway and sensor bit depth, as described in Section 12. This representation preserves precision while improving storage efficiency and compatibility with standard remote sensing tools.

In addition to surface reflectance, ACOMP generates a set of auxiliary products that describe the atmospheric state and retrieval quality. These include:

- **Aerosol Optical Depth (AOD) Map**, representing the estimated aerosol loading across the scene
- **Uncertainty Map**, providing a per-pixel estimate of reflectance sensitivity to atmospheric variability
- **Haze Classification (Browse)**, offering a qualitative visualization of atmospheric conditions
- **Metrics File**, documenting acquisition geometry, atmospheric parameters, calibration inputs, and processing statistics

All outputs are written in GeoTIFF format and preserve geolocation and metadata consistency with the input imagery.

These outputs collectively provide both the corrected reflectance product and the contextual information necessary for quantitative analysis and quality assessment. The inclusion of atmospheric and uncertainty layers enables users to interpret the reliability of the correction and supports downstream applications that require error-aware data. These outputs are not necessarily provided with operational data.

Table 4. Algorithm Outputs

Output	Description
Surface Reflectance	Per-pixel surface reflectance for each spectral band; stored as a scaled integer
Aerosol Optical Depth (AOD) Map	Retrieved aerosol optical depth representing atmospheric conditions
Uncertainty Map	Per-pixel estimate of reflectance uncertainty derived from sensitivity to atmospheric parameters
Haze Classification (Browse)	Visualization of haze conditions derived from AOD ranges
Metrics File	Summary of processing inputs, atmospheric parameters, geometry, and algorithm diagnostics
Output Imagery (Formatted)	GeoTIFF output preserving spatial reference and metadata structure

4. Algorithm Overview & Processing Framework

4.1 Algorithm Overview

The Atmospheric Compensation (ACOMP) algorithm converts calibrated top-of-atmosphere (TOA) measurements into surface reflectance using a radiative transfer–based framework that represents atmospheric scattering and absorption processes through precomputed lookup tables (LUTs). The algorithm combines sensor metadata, scene geometry, ancillary atmospheric information, and radiative transfer modeling to estimate atmospheric state parameters and retrieve surface reflectance. It is designed to operate across a wide range of optical satellite sensors with differing spectral configurations, including multispectral and panchromatic systems.

The algorithm is implemented in a modular fashion to support multiple sensors and product types. Sensor-specific differences in metadata, spectral response, and calibration are handled through dedicated preprocessing and parameter selection steps. Atmospheric correction is performed using a hybrid approach that combines radiative transfer modeling, implemented via LUT interpolation, with empirical constraints derived from scene content. This design maintains physical consistency while allowing the algorithm to adapt to varying observational and atmospheric conditions.

4.2 Processing Workflow

ACOMP processing begins with ingestion of the input image and associated metadata. The algorithm identifies the sensor type, spectral configuration, and data format, and converts the input into a standardized internal representation. This may include band stacking, mosaicking (e.g., Sentinel-2 granules), and conversion to a consistent interleave format.

Metadata are parsed to extract acquisition time, solar and sensor geometry, calibration parameters, spectral response functions, and scene extent. From these inputs, additional physical quantities are derived, including Earth–Sun distance and scattering geometry, which define the radiative transfer conditions for the scene.

Radiometric calibration is applied to convert digital numbers to top-of-atmosphere (TOA) radiance using sensor-specific gain and offset parameters.

Initial atmospheric conditions are established using ancillary datasets, including surface elevation, atmospheric profile type, aerosol properties, and column water vapor. These parameters define the starting point for atmospheric correction and guide selection of the radiative transfer model.

For sensors with appropriate spectral bands, water vapor may be refined using band-ratio methods. A common approach uses absorption-sensitive and reference bands in the near-infrared (e.g., ~940 nm absorption band relative to a nearby non-absorbing band such as ~865 nm or ~820 nm), allowing estimation of column water vapor through differential absorption. When such bands are not available, ancillary climatological values are retained.

Atmospheric parameters required for the inversion, including path radiance and transmittance, are obtained from precomputed lookup tables (LUTs) or optional MODTRAN simulations. These LUTs are generated across a discretized parameter space, including aerosol optical depth (AOD), geometry, and elevation, and are interpolated during processing.

A scene-level aerosol optical depth (AOD) is estimated using image-based methods and radiative transfer consistency checks. This estimate serves as the primary atmospheric constraint for the scene. Spatial refinement of AOD may be performed depending on processing configuration.

Surface reflectance is then computed for each pixel and spectral band using the radiative transfer inversion. The inversion incorporates interpolated atmospheric parameters, including AOD-dependent path radiance and transmittance, and includes adjacency-adjusted radiance terms to account for neighborhood effects.

An optional uncertainty estimate is generated by perturbing AOD within a bounded range and evaluating the sensitivity of the retrieved reflectance.

Final outputs include surface reflectance and optional auxiliary products such as AOD, uncertainty, haze classification, and processing metrics. Output values are scaled according to

the selected format and written to GeoTIFF. Temporary files are removed upon completion.

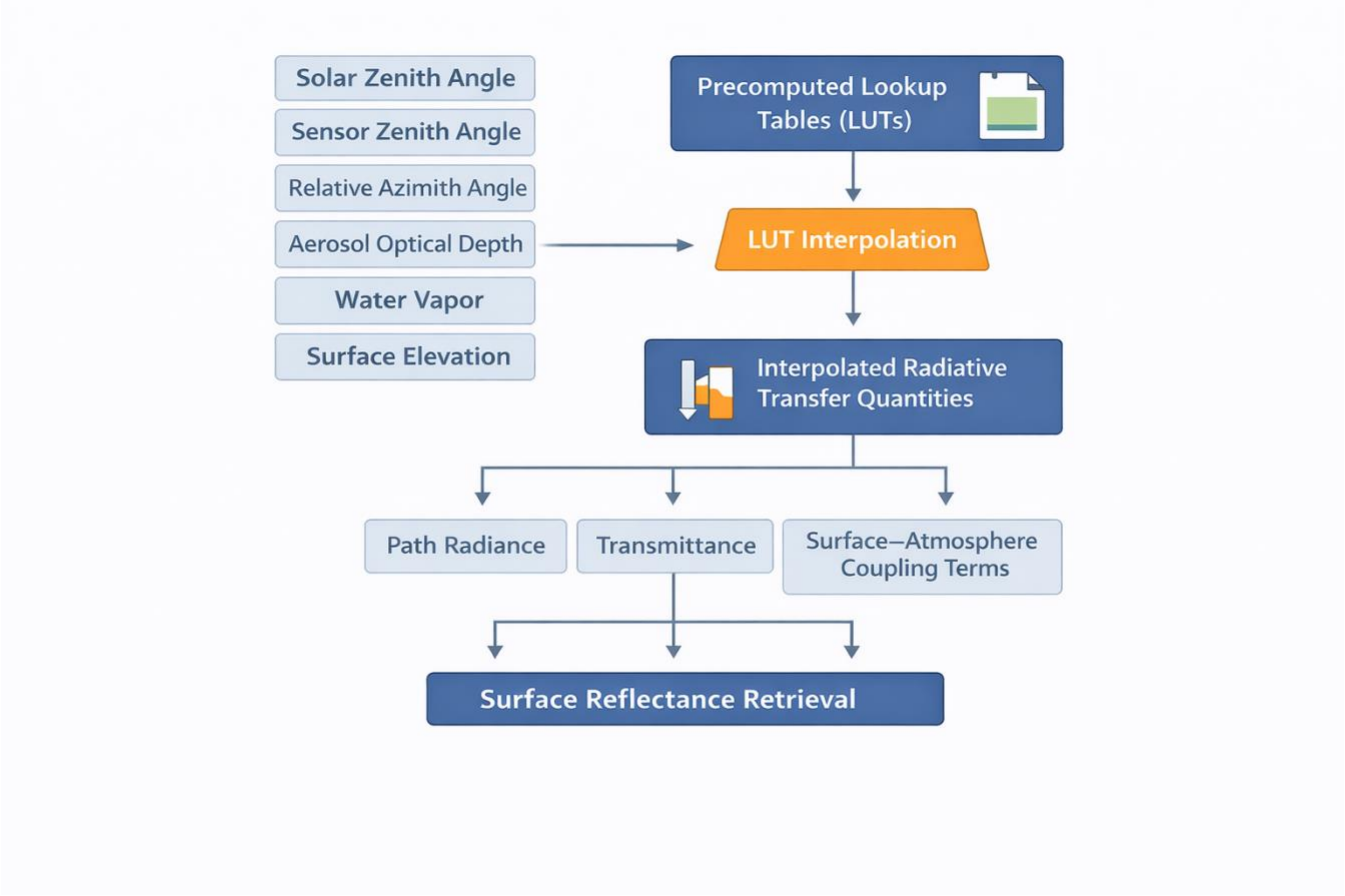

Figure 2. LUT-based radiative transfer workflow in ACOMP. Scene-dependent inputs are used to interpolate atmospheric parameters from precomputed lookup tables, which are then applied to retrieve surface reflectance.

4.3 Spatially Adaptive Atmospheric Correction

ACOMP employs a spatially adaptive atmospheric correction framework in which atmospheric properties are estimated primarily at the scene level and optionally refined to account for spatial variability. This approach provides a balance between physical consistency and robustness, particularly in heterogeneous scenes where fully pixel-wise atmospheric retrieval can be unstable.

Aerosol optical depth (AOD) is first estimated at the scene level using a combination of complementary image-based methods. Dark Object Subtraction (DOS) analysis is used to identify pixels with very low surface reflectance, such as deep water, dense vegetation, or shadowed

areas. These pixels are assumed to have near-zero reflectance in visible bands, allowing atmospheric path radiance to be approximated from the observed signal:

$$L_{TOA} \approx L_{path} \text{ for } \rho_s \lesssim 0.02\text{–}0.05 \quad [1]$$

Empirical reflectance thresholds are used to identify suitable dark targets and exclude anomalous pixels.

Additional constraints are provided by vegetation-based methods, in which pixels are classified using spectral indices such as the Normalized Difference Vegetation Index (NDVI):

$$NDVI = \frac{NIR-Red}{NIR+Red} \quad [2]$$

Pixels with high NDVI exhibit predictable spectral behavior, particularly low reflectance in shorter wavelengths relative to near-infrared bands, and are therefore useful for separating aerosol scattering from surface reflectance contributions.

The AOD estimate is further refined using radiative transfer consistency checks, in which candidate AOD values are evaluated by comparing observed radiance with LUT-derived radiative transfer simulations:

$$\tau_a = \arg\ \min\ |\ L_{obs} - L_{model}(\tau)\ |\ \ [3]$$

Solutions are selected based on minimizing residual differences while satisfying physically realistic bounds. These bounds are enforced using critical radiance and reflectance thresholds, which are empirically defined based on sensor characteristics and expected radiometric behavior.

Radiative transfer lookup tables used in this process are generated over a discretized aerosol optical depth grid spanning clear to moderately hazy conditions:

$$\tau_a \in [0,1+] \text{with sampling intervals} \approx 0.01\text{–}0.05 \quad [4]$$

This fine sampling enables stable interpolation of radiative transfer quantities, including path radiance and atmospheric transmittance.

When spatial refinement is enabled, local AOD estimates are derived over subregions of the scene using the same spectral and radiative transfer constraints applied in the global retrieval. These localized estimates are interpolated across the scene using smoothing approaches such as regression-based interpolation or kriging:

$$\tau_a(x, y) = \sum_i w_i\,(x, y)\,\tau_{a,i} \quad [5]$$

where w_i are distance- and confidence-weighted interpolation coefficients. The resulting AOD field is constrained to be spatially continuous and physically consistent while avoiding instability in low-information regions. In the current operational configuration, ACOMP primarily relies on a scene-based AOD estimate with limited spatial refinement.

Surface reflectance is then computed for each pixel using atmospheric parameters interpolated from the lookup tables at the retrieved AOD. Although the atmospheric state is largely constrained at the scene level, pixel-level variability is preserved through differences in viewing geometry, illumination, and surface reflectance.

Adjacency effects are addressed through spatial smoothing and effective neighborhood radiance terms rather than explicit radiative transfer kernel modeling. These approximations reduce high-frequency artifacts while maintaining computational efficiency.

This spatially adaptive design reflects a key tradeoff in the algorithm: prioritizing stability and robustness over fully independent per-pixel atmospheric retrieval. By anchoring the solution to a scene-based atmospheric state while allowing limited spatial variation, ACOMP achieves consistent and physically realistic correction across diverse imaging conditions.

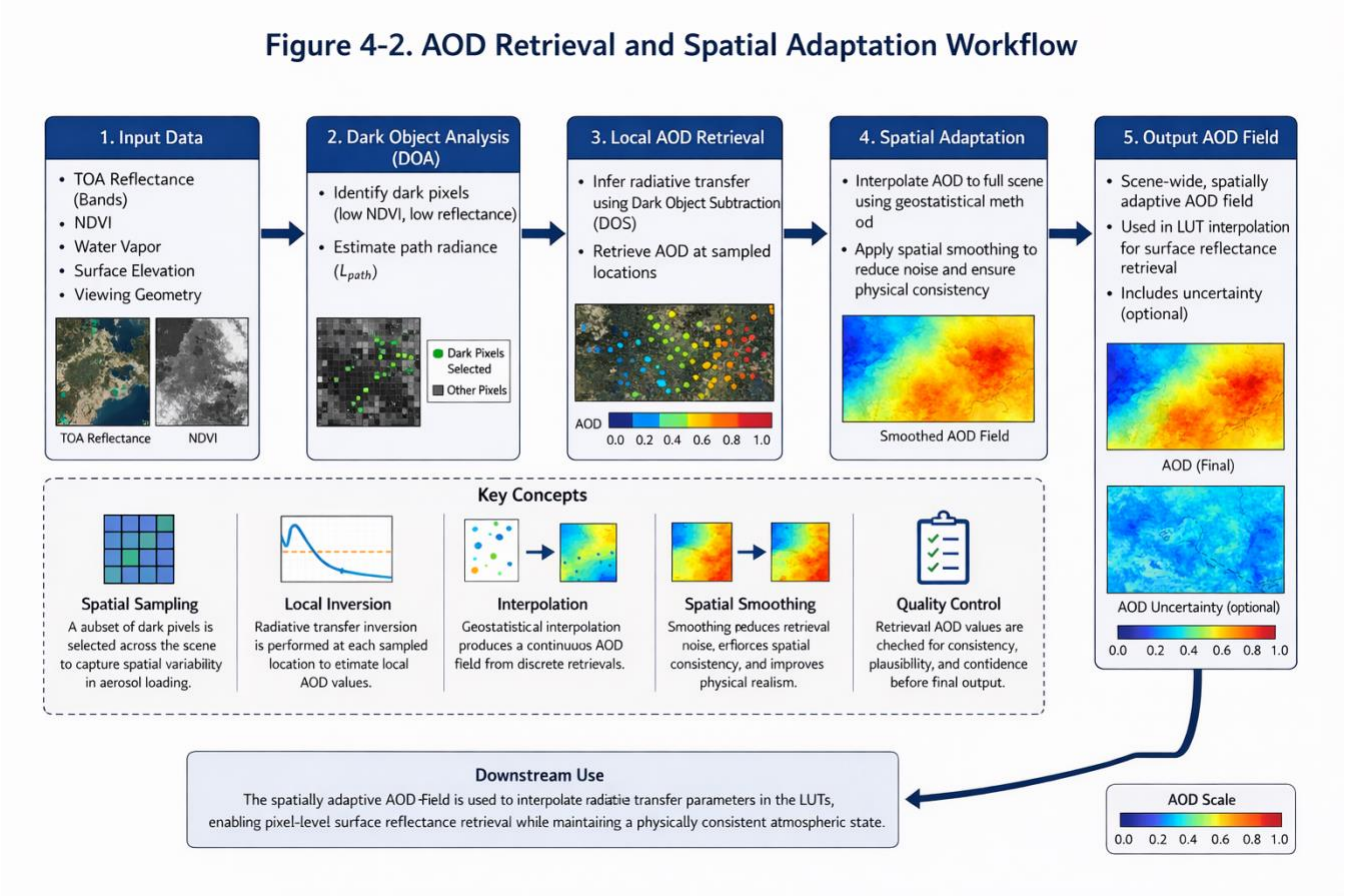

Figure 3. AOD Estimation and Spatial Interpolation Framework. Conceptual illustration of aerosol optical depth (AOD) estimation and spatial refinement in ACOMP. Initial AOD estimates are derived from dark-object Subtraction (DOS) analysis and vegetation-based constraints. These estimates are evaluated against a discretized LUT-based AOD grid and refined through spatial interpolation to produce a continuous and physically consistent AOD field used in surface reflectance retrieval.

5. Radiative Transfer Formulation

5.1 Radiative Transfer Implementation in ACOMP

The ACOMP algorithm is based on a radiative transfer framework that describes the interaction of solar radiation with the atmosphere and the Earth's surface. Satellite sensors measure top-of-atmosphere (TOA) radiance, which includes contributions from atmospheric scattering (path radiance), surface-reflected radiance attenuated by atmospheric transmission, and radiance scattered from neighboring pixels (adjacency effects). The objective of atmospheric correction is to separate these components and recover surface reflectance.

In ACOMP, the observed TOA radiance can be expressed as:

$$L_{TOA}(\lambda) = L_{path}(\lambda) + L_{adj}(\lambda) + T_v(\lambda)\,\frac{E_0(\lambda)\cos(\theta_s)}{\pi}\,\rho_s(\lambda)\,T_s(\lambda) \quad [6]$$

where $L_{TOA}$is the radiance measured at the sensor, $L_{path}$is atmospheric path radiance, $L_{adj}$is the adjacency radiance contribution from surrounding pixels, $T_s$and $T_v$are the downward and upward atmospheric transmittance terms, respectively, $E_0$is the extraterrestrial solar irradiance, $\theta_s$is the solar zenith angle, and $\rho_s$is the surface reflectance. This formulation follows standard radiative transfer representations used in atmospheric correction models (e.g., Vermote et al., 1997; Tanré et al., 1981).

In practice, ACOMP does not compute these radiative transfer quantities through on-the-fly simulations for each pixel. Instead, atmospheric parameters such as path radiance, transmittance, and adjacency contributions are obtained from precomputed lookup tables (LUTs) derived from radiative transfer simulations (e.g., MODTRAN). These LUTs provide atmospheric quantities as functions of geometry, atmospheric state, and aerosol optical depth, enabling efficient interpolation during processing while preserving consistency with radiative transfer physics.

The atmospheric parameters used in this inversion are derived using the spatially adaptive retrieval approach described in Section 4.

A key component of the framework is the estimation of aerosol optical depth (AOD), which strongly influences both atmospheric scattering and transmittance. ACOMP retrieves AOD using a scene-based approach that compares observed radiance with LUT-based radiative transfer predictions. Additional atmospheric parameters, including water vapor, may be optionally refined using spectral information when suitable bands are available.

Through this combination of radiative transfer modeling, LUT interpolation, and scene-based parameter estimation, ACOMP produces surface reflectance estimates that are consistent across varying atmospheric conditions. Optional outputs include spatially resolved AOD fields and uncertainty estimates that characterize sensitivity to atmospheric variability.

5.2 Atmospheric State Characterization

Accurate atmospheric correction requires characterization of the atmospheric state governing the propagation of solar radiation between the Sun, the surface, and the sensor. In ACOMP, this characterization is performed using a hybrid approach that combines ancillary datasets with scene-based parameter estimation within a radiative transfer–based framework.

Key atmospheric parameters include aerosol optical depth (AOD), column water vapor, atmospheric pressure (derived from elevation), and an atmospheric profile describing temperature and gas composition. Surface elevation is obtained from an internal digital elevation model (DEM), from which a representative mean elevation is computed for the scene. This value is used to estimate surface pressure and adjust atmospheric path length in the radiative transfer calculations.

Atmospheric profiles and initial atmospheric conditions are selected from climatological datasets rather than retrieved from external numerical weather models. The algorithm determines an appropriate standard atmospheric model (e.g., tropical, mid-latitude, subarctic) based on scene location and time of year. Initial estimates of aerosol optical depth and water vapor are similarly obtained from climatological databases and serve as starting conditions for the correction.

AOD is subsequently refined using a scene-based retrieval approach that compares observed radiance with lookup table (LUT)-based radiative transfer predictions across a range of candidate values. This allows the algorithm to adjust atmospheric conditions to best match the observed signal. Depending on configuration, ACOMP estimates AOD at a scene-wide level with optional spatial refinement, as described in Section 4.

Water vapor may also be refined using image-based estimation when suitable spectral bands are available (e.g., near-infrared absorption features). When such bands are not present, the ancillary estimate is retained. Molecular (Rayleigh) scattering is not retrieved but is computed deterministically from atmospheric pressure and geometry within the radiative transfer framework.

Overall, ACOMP characterizes the atmospheric state through a combination of climatological initialization, radiative transfer–based modeling implemented via lookup tables, and scene-dependent refinement. This approach enables consistent and robust atmospheric correction without requiring external in situ measurements.

5.3 Molecular Scattering (Rayleigh Correction)

Molecular (Rayleigh) scattering arises from the interaction of electromagnetic radiation with atmospheric gases whose sizes are much smaller than the wavelength of the incident radiation. In the Earth's atmosphere, the primary molecular scatterers are nitrogen (N_2) and oxygen (O_2). Because the scattering efficiency varies approximately with the inverse fourth power of wavelength (λ^{-4}), Rayleigh scattering is strongest at shorter wavelengths, particularly in the blue portion of the spectrum. This wavelength dependence explains both the blue color of the sky and the strong atmospheric contribution observed in visible satellite measurements.

The magnitude of Rayleigh scattering is characterized by the Rayleigh optical depth, $\tau_R(\lambda)$, which depends on wavelength and atmospheric pressure. In ACOMP, the Rayleigh optical depth is adjusted for surface elevation through its dependence on pressure:

$$\tau_R(\lambda) = \frac{P}{P_0} \cdot \tau_{R0}(\lambda) \quad [7]$$

where $P$is the surface atmospheric pressure, $P_0$is the standard atmospheric pressure, and $\tau_{R0}(\lambda)$is the Rayleigh optical depth at standard pressure for wavelength λ. The wavelength dependence of $\tau_{R0}(\lambda)$follows the inverse fourth-power relationship, with additional corrections for refractive index and depolarization effects (Bodhaine et al., 1999).

Surface pressure is derived from elevation using the hydrostatic approximation of the atmosphere. Under standard assumptions, pressure as a function of height can be expressed as:

$$P(z) = P_0 \exp\left(-\frac{gz}{RT}\right) \quad [8]$$

where z is elevation, g is gravitational acceleration, R is the specific gas constant for dry air, and T is atmospheric temperature. This relationship reflects the decrease in atmospheric density with altitude and allows the algorithm to account for variations in molecular scattering due to changes in pressure and optical path length. Uncertainty in elevation, and therefore in derived pressure, propagates directly into Rayleigh optical depth and contributes to reflectance uncertainty, as described in Section 8.

Rayleigh scattering contributes to both atmospheric path radiance and transmittance terms in the radiative transfer equation. In ACOMP, these contributions are computed using precomputed radiative transfer lookup tables (LUTs), which incorporate molecular scattering effects as a function of wavelength, geometry, and atmospheric state. The Rayleigh component is separated from aerosol scattering during atmospheric parameter estimation, enabling independent characterization of molecular and aerosol contributions.

Accurate representation of Rayleigh scattering is critical for surface reflectance retrieval, particularly in shorter wavelengths where its contribution is largest. Errors in pressure estimation or molecular scattering parameterization can propagate into reflectance uncertainty, although these effects are generally smaller than aerosol-related uncertainties under most conditions.

5.4 Aerosol Optical Depth Retrieval

Aerosols represent one of the largest sources of uncertainty in atmospheric correction, as they strongly influence scattering and atmospheric path radiance. Aerosol scattering arises from the interaction of solar radiation with suspended particles in the atmosphere whose sizes are comparable to or larger than the wavelength of visible light. These particles include dust, smoke, sea salt, sulfates, and other natural or anthropogenic particulates. Unlike Rayleigh scattering, aerosol scattering exhibits a weaker wavelength dependence and often produces strongly forward-peaked scattering.

The magnitude and angular distribution of aerosol scattering are governed by particle properties such as size distribution, complex refractive index, and particle shape. These processes are commonly described using Mie scattering theory, in which scattering behavior is determined by the particle size parameter:

$$x = \frac{2\pi r}{\lambda} \qquad [9]$$

where r is particle radius and λ is wavelength. These scattering properties are incorporated into radiative transfer models through aerosol phase functions and extinction coefficients, which together determine the aerosol contribution to atmospheric attenuation.

The integrated effect of aerosol scattering and absorption along the atmospheric path is quantified by aerosol optical depth (AOD), τ_a. In ACOMP, AOD is treated as the primary parameter controlling aerosol effects and is retrieved using a scene-based approach that leverages spectral and radiative transfer consistency.

At a conceptual level, AOD is estimated by comparing observed top-of-atmosphere (TOA) radiance with radiative transfer simulations across a range of candidate AOD values. The optimal value is selected as the one that minimizes the difference between observed and modeled radiance:

$$\tau_a = \arg\ \min\ |\ L_{obs} - L_{model}(\tau)\ | \qquad [10]$$

where L_{obs} is the observed radiance and $L_{model}(\tau)$ is the modeled radiance as a function of aerosol optical depth.

In practice, the ACOMP implementation extends beyond a simple global minimization. The algorithm first derives a scene-based AOD estimate using multiple complementary approaches, including dark-object analysis, vegetation-based constraints, and radiative transfer consistency

checks. These independent estimates are combined using confidence-weighted metrics to produce a robust initial AOD value.

Following this, the algorithm supports optional spatial refinement of AOD to better represent heterogeneous atmospheric conditions. Local AOD values may be estimated over subregions of the image using spectral constraints and surface-type information, and are then interpolated across the scene using smoothing techniques such as kriging or regression-based methods. This ensures that the resulting AOD field is spatially continuous and physically consistent, while avoiding instability in regions with limited retrieval information. In the current operational configuration, ACOMP primarily relies on a scene-based AOD estimate, with spatial adaptation applied in a constrained manner.

The retrieval relies on spectral bands that are sensitive to atmospheric scattering while minimizing surface reflectance contamination, particularly in the visible and near-infrared regions. Additional constraints based on surface type and radiometric behavior are applied to reduce ambiguity between aerosol effects and surface reflectance.

The retrieved AOD is used to parameterize aerosol scattering within the radiative transfer framework, influencing both atmospheric path radiance and transmittance terms in the surface reflectance inversion. Accurate estimation of AOD is therefore critical for reliable atmospheric correction. Uncertainty in AOD retrieval represents the dominant contributor to surface reflectance error, as described in Section 8.

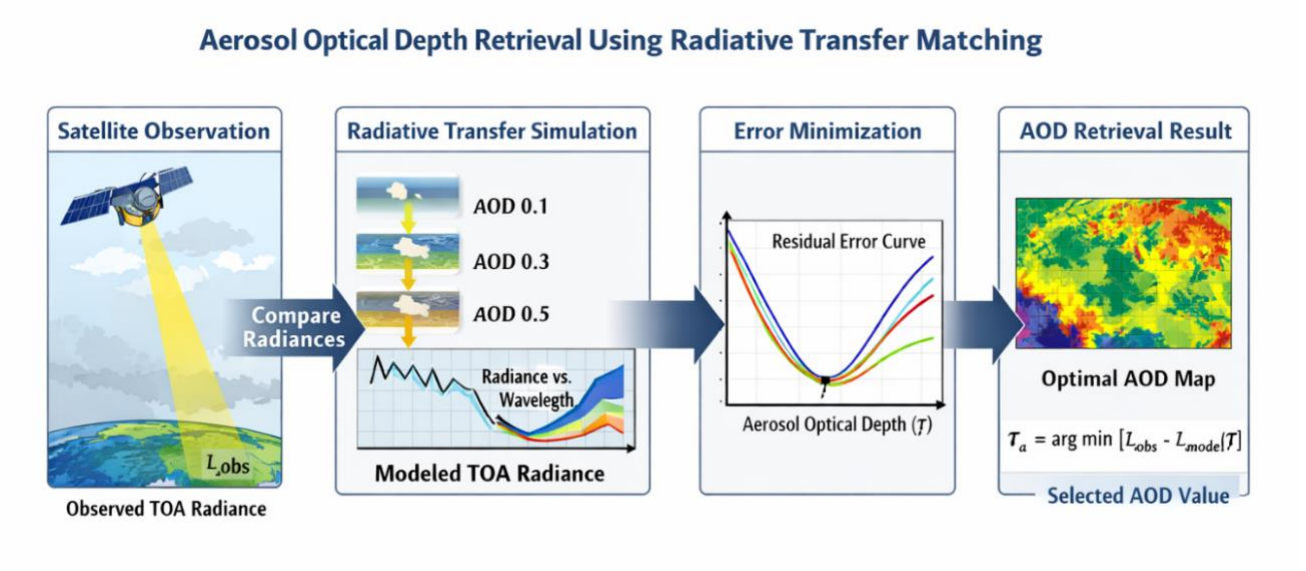

Figure 4. Conceptual diagram illustrating aerosol optical depth retrieval using radiative transfer matching.

5.5 Gas Absorption Correction

Atmospheric absorption by trace gases reduces both the incoming solar irradiance reaching the Earth's surface and the reflected radiance observed by the satellite sensor. The primary absorbing gases affecting optical satellite observations in the visible and near-infrared spectral regions are water vapor (H_2O), ozone (O_3), and molecular oxygen (O_2). These gases exhibit distinct, wavelength-dependent absorption features that must be accounted for when retrieving surface reflectance from top-of-atmosphere (TOA) radiance measurements.

Ozone absorption is most significant in the ultraviolet and portions of the visible spectrum, particularly within the Chappuis bands (~450–750 nm), and therefore affects several blue and green spectral bands. Molecular oxygen contributes narrow absorption features, most notably the O_2-A band near 760 nm. Water vapor is the dominant absorbing gas in the near-infrared and shortwave infrared regions, with strong absorption bands centered near approximately 720 nm, 820 nm, 940 nm, and 1130 nm.

The magnitude of gaseous absorption is governed by wavelength-dependent absorption coefficients and the column abundance of each gas species. In atmospheric correction, gaseous absorption can be conceptually represented as a multiplicative attenuation of the radiance signal through atmospheric transmittance:

$$T_{gas}(\lambda) = e^{-k(\lambda)\,u} \quad [11]$$

where $k(\lambda)$ is the absorption coefficient at wavelength λ, and u is the column abundance of the absorbing gas.

Gas absorption contributes directly to the atmospheric transmittance terms T_s and T_v in the surface reflectance inversion described in Section 5.2. Conceptually, the total atmospheric transmittance may be expressed as:

$$T(\lambda) = T_{Rayleigh}(\lambda) \cdot T_{aerosol}(\lambda) \cdot T_{gas}(\lambda) \quad [12]$$

where molecular scattering, aerosol extinction, and gas absorption contribute multiplicatively to the total attenuation of radiation.

Within ACOMP, however, these components are not computed independently at runtime. Instead, gaseous absorption is accounted for implicitly through precomputed radiative transfer lookup tables (LUTs) or MODTRAN-based simulations. These LUTs incorporate spectroscopic databases and atmospheric profiles to represent gas absorption effects across the sensor

spectral response functions. As a result, gas absorption is embedded within the atmospheric parameters used during surface reflectance retrieval, including path radiance, transmittance, and coupling terms.

Water vapor receives additional attention in the algorithm due to its strong spatial and temporal variability. As described in Section 3.2, water vapor is primarily obtained from ancillary atmospheric datasets and used to parameterize gas absorption within the LUT framework. In processing configurations where sufficient spectral information is available, limited scene-based refinement of water vapor may be applied; however, ACOMP does not rely on a full independent water vapor retrieval. Ozone and oxygen absorption are represented using standard atmospheric assumptions within the LUTs.

Accurate characterization of gas absorption, particularly water vapor, is important for surface reflectance retrieval in bands affected by absorption features. Errors in gas absorption modeling primarily impact specific spectral regions and are generally smaller than aerosol-related uncertainties but can become significant within strong absorption bands. These effects contribute to reflectance uncertainty as described in Section 8.

5.6 Surface Reflectance Retrieval

Once atmospheric parameters have been estimated, the ACOMP algorithm retrieves surface reflectance by removing atmospheric contributions from the observed top-of-atmosphere (TOA) radiance. This process accounts for atmospheric path radiance, transmittance, and adjacency effects derived from the radiative transfer framework.

In its general form, surface reflectance is expressed as:

$$\rho_s(\lambda) = \frac{\pi\left[L_{TOA}(\lambda) - L_{path}(\lambda) - L_{adj}(\lambda)\right]}{E_0(\lambda)\cos(\theta_s)\, T_s(\lambda)\, T_v(\lambda)} \qquad [13]$$

where:

L_{TOA}— Top-of-atmosphere radiance (affected by radiometric calibration uncertainty)

L_{path}— Atmospheric path radiance (driven by aerosol and molecular scattering)

L_{adj}— Adjacency radiance contribution (spatial scattering from neighboring pixels)

T_s, T_v— Downward and upward atmospheric transmittance (affected by aerosol, gas absorption, and atmospheric profile assumptions)

E_0— Extraterrestrial solar irradiance (systematic calibration input)

θ_s— Solar zenith angle (geometry-dependent)

ρ_s— Surface reflectance

This formulation directly links the retrieved reflectance to the atmospheric and radiometric components described in Section 8.

The retrieval is performed on a pixel-by-pixel basis using atmospheric parameters interpolated from lookup tables at the retrieved aerosol optical depth (AOD). Although the atmospheric state is constrained at the scene level, pixel-level variability is preserved through differences in viewing geometry, illumination, and surface properties.

When multiple aerosol models are considered, the algorithm combines candidate solutions using a weighting scheme based on retrieval confidence and AOD magnitude.

The algorithm assumes a Lambertian surface reflectance model, which simplifies the inversion by treating reflectance as isotropic. While natural surfaces exhibit bidirectional reflectance distribution function (BRDF) behavior, this approximation is generally sufficient for most land surface applications and is widely used in operational atmospheric correction algorithms. Deviations from this assumption contribute to reflectance uncertainty as described in Section 8.

6. Algorithm Implementation

6.1 Lookup Tables

Radiative transfer modeling is a central component of atmospheric correction; however, direct execution of full physics-based models such as MODTRAN for every pixel would be computationally prohibitive for large-scale image processing. To address this, ACOMP relies primarily on precomputed lookup tables (LUTs) that encapsulate radiative transfer solutions across a representative range of atmospheric and geometric conditions. This approach enables efficient retrieval of atmospheric parameters during processing while preserving consistency with rigorous radiative transfer theory.

The LUTs are generated using MODTRAN 5.0 by simulating top-of-atmosphere radiance and associated atmospheric quantities over a multidimensional parameter space. Key input dimensions include solar zenith angle, sensor viewing geometry, relative azimuth angle, aerosol optical depth (AOD), and surface elevation. These parameters are selected to span the range of conditions typically encountered in optical satellite imagery.

Each LUT entry stores the radiative transfer components required for surface reflectance retrieval, including atmospheric path radiance, downward and upward transmittance, and related coupling terms used in the inversion of the radiative transfer equation. The LUTs are therefore not simple reflectance lookups, but compact representations of the forward radiative transfer model evaluated over discretized atmospheric states.

During processing, ACOMP queries these multidimensional LUTs using scene-specific inputs derived from image metadata and internal atmospheric retrievals. These inputs include solar and

sensor geometry, estimated aerosol optical depth from the scene-based retrieval, and surface elevation obtained from a digital elevation model. By interpolating within the LUT parameter space, the algorithm reconstructs the atmospheric terms required for each pixel without invoking a full radiative transfer simulation.

Although LUT-based processing is the default operational mode, ACOMP retains the capability to generate radiative transfer solutions dynamically using MODTRAN when higher fidelity is required. This option is typically reserved for specialized analyses due to its significantly higher computational cost.

The LUT parameter space is designed to encompass realistic observation conditions. Typical ranges include solar zenith angles from 0 to 75 degrees, sensor zenith angles from 0 to 60 degrees, relative azimuth angles from 0 to 180 degrees, aerosol optical depth values spanning clear to highly turbid conditions (extending beyond 1.0 where needed for robustness), and surface elevations from sea level to approximately 5 km. This coverage ensures stable interpolation across diverse atmospheric and geographic environments.

6.2 Interpolation and Parameter Selection

The ACOMP algorithm derives atmospheric correction parameters by querying and interpolating within precomputed radiative transfer lookup tables (LUTs). These LUTs are discretely sampled across key dimensions including aerosol optical depth (AOD), solar and sensor geometry, relative azimuth, and surface elevation. Because the exact combination of conditions for a given pixel will generally fall between discrete LUT grid points, interpolation is required to obtain physically consistent atmospheric parameters.

Interpolation in ACOMP is primarily performed along the aerosol optical depth dimension, which is the dominant variable controlling atmospheric scattering. During LUT generation, radiative transfer outputs are computed at a set of discrete AOD values. In some implementations, smoothing or spline-based interpolation may be applied during LUT construction to ensure that radiative transfer quantities vary smoothly with AOD. At runtime, the algorithm performs linear interpolation between adjacent AOD nodes to estimate atmospheric parameters corresponding to the retrieved aerosol optical depth for each pixel.

Formally, for a given atmospheric quantity Q (e.g., path radiance or transmittance), the interpolated value is computed as:

$$Q(\tau) = Q(\tau_i) + \frac{\tau - \tau_i}{\tau_{i+1} - \tau_i}[Q(\tau_{i+1}) - Q(\tau_i)] \quad [14]$$

where τ is the retrieved aerosol optical depth, and τ_i and τ_{i+1} are the bounding LUT nodes.

Other dimensions of the LUT, including solar zenith angle, sensor viewing angle, relative azimuth, and surface elevation, are typically handled through nearest-neighbor selection or discrete binning rather than continuous interpolation. The appropriate LUT subset is selected based on scene-specific metadata and ancillary inputs, ensuring consistency between the radiative transfer simulations and the observed acquisition geometry.

This hybrid approach—combining interpolation along the aerosol dimension with discrete selection across geometric and environmental parameters—provides an efficient balance between computational performance and physical fidelity. It enables pixel-level adaptation to spatially varying aerosol conditions while maintaining tractable processing times for large imagery datasets.

6.3 Implementation of Spatially Adaptive Processing

ACOMP performs surface reflectance retrieval at the pixel level while constraining atmospheric parameters primarily at the scene level. Atmospheric state variables, particularly aerosol optical depth (AOD), are derived using the spatially adaptive retrieval approach described in Section 4.3 and then applied during pixel-wise radiative transfer inversion.

In the current implementation, a scene-based AOD estimate serves as the primary atmospheric constraint. Optional spatial refinement, when enabled, provides a smoothed AOD field derived from localized retrievals and interpolation methods. These AOD values are used to query and interpolate within the radiative transfer lookup tables (LUTs), ensuring that atmospheric parameters remain physically consistent across the scene.

Surface reflectance is computed independently for each pixel using geometry-specific radiative transfer quantities, including viewing angles, solar illumination, and surface radiance. As a result, spatial variability in the final reflectance product arises from differences in geometry and surface properties, while atmospheric variability is represented in a controlled and smoothed manner through the AOD field.

This design reflects a balance between physical realism and computational stability. By anchoring the atmospheric solution to a smoothly varying AOD estimate, the algorithm avoids noise and instability associated with fully independent pixel-wise atmospheric retrievals, particularly in low-signal or heterogeneous regions.

Although the framework supports fully spatially varying atmospheric parameters, the current implementation applies spatial adaptation in a constrained manner. Consequently, performance may be reduced in scenes with strong spatial gradients in aerosol loading or haze. Future enhancements may incorporate more explicit spatial modeling of atmospheric variability to improve performance under such conditions.

6.4 Adjacency Effects Handling

Adjacency effects arise from lateral atmospheric scattering, whereby photons reflected from neighboring surfaces are scattered into the sensor's line of sight. As a result, the observed top-of-atmosphere (TOA) radiance includes contributions not only from the target surface and atmospheric path radiance, but also from surrounding pixels. This effect is most pronounced in scenes with strong spatial contrast (e.g., bright targets adjacent to dark surfaces) and under elevated aerosol loading, where scattering is enhanced.

In a radiative transfer framework, adjacency can be represented as an additional radiance term:

$$L_{TOA}(x,y) = L_{path}(x,y) + L_{adj}(x,y) + L_{surf}(x,y) \qquad [15]$$

where L_{adj} denotes the adjacency radiance contribution. This term can be approximated as a spatially weighted contribution from neighboring surface radiance:

$$L_{adj}(x,y) \approx \iint K(x-x', y-y')\, L_{surf}(x',y')\, dx'\, dy' \qquad [16]$$

or, in discrete form,

$$L_{adj,i} \approx \sum_{j \neq i} w_{ij}\ L_{surf,j} \qquad [17]$$

where K or w_{ij} represents a distance-dependent atmospheric scattering kernel governed by aerosol properties, viewing geometry, and atmospheric conditions.

Adjacency is represented in the radiative transfer formulation but is not explicitly solved via full radiative transfer kernel in this current implementation. Instead, its impact is partially mitigated through spatially adaptive atmospheric parameter estimation and smoothing of the aerosol optical depth (AOD) field. This approximation is broadly consistent with operational atmospheric correction approaches, which often mitigate adjacency effects through spatial smoothing and simplified parameterizations rather than explicit radiative transfer kernel modeling (e.g., Vermote et al., 1997; Tanré et al., 1981). These approaches reduce high-frequency spatial variability and limit amplification of adjacency-related artifacts, particularly in heterogeneous scenes.

Despite these mitigation strategies, residual adjacency effects may persist, especially in high-resolution imagery with strong reflectance gradients or under hazy conditions. These effects represent a known limitation of the current implementation and motivate future enhancements incorporating explicit adjacency correction methods based on radiative transfer kernels or spatial deblurring approaches.

7. Output and Quality Assessment

7.1 Output Surface Reflectance Product

The final output of the ACOMP algorithm is a surface reflectance product that represents the spectral reflectance of the Earth's surface after removal of atmospheric effects. These values correspond to the reflectance that would be observed under idealized, atmosphere-free conditions and are provided for each spectral band of the input sensor. As such, the product is intended to support consistent quantitative analysis across scenes acquired under varying illumination and atmospheric conditions.

For efficient storage and compatibility with standard data formats, surface reflectance is typically represented as scaled integers rather than floating-point values. The scaling is applied according to

$$\rho_{scaled} = \rho_s \times S \qquad [18]$$

where ρ_s is the retrieved surface reflectance and S is a predefined scale factor. This approach preserves precision while reducing file size and maintaining interoperability with common remote sensing tools.

In addition to surface reflectance, the algorithm generates several ancillary outputs that provide information about atmospheric conditions and retrieval quality. These include an aerosol optical depth (AOD) product, which characterizes the spatial distribution of atmospheric aerosols across the scene, and quality flags that indicate retrieval confidence and potential issues such as haze or other atmospheric artifacts. Together, these outputs form a comprehensive dataset that enables both scientific analysis and quality assessment of the corrected imagery.

7.2 Quality Assessment

Quality assessment in ACOMP is primarily derived from internally computed metrics that reflect the stability and reliability of the atmospheric retrieval, rather than from externally supplied

quality flags. During processing, the algorithm evaluates the consistency of aerosol optical depth (AOD) retrievals, the spatial variability of the solution, and the sensitivity of the inversion to uncertainties in atmospheric parameters. These diagnostics are used to quantify confidence in the retrieved surface reflectance.

A key component of the quality assessment is the generation of an AOD confidence field, which reflects the robustness of the aerosol retrieval at each location. This confidence is based on multiple factors, including agreement between independent retrieval methods (e.g., dark-object, vegetation-based, and radiative transfer consistency approaches), signal-to-noise characteristics, and spectral consistency checks. Areas with low confidence are handled conservatively through spatial smoothing or fallback to global AOD estimates.

In addition, ACOMP produces an explicit uncertainty estimate for surface reflectance. This uncertainty is derived by perturbing the AOD within a bounded range and evaluating the resulting variation in retrieved reflectance. The magnitude of this variation provides a per-pixel estimate of retrieval sensitivity, which serves as a practical indicator of product reliability.

The algorithm also generates diagnostic outputs such as haze severity classification and AOD spatial distribution, which provide contextual information about atmospheric conditions across the scene. These diagnostics help users interpret the quality of the correction, particularly in cases of heavy haze or spatially variable aerosols.

It is important to note that ACOMP does not inherently perform explicit cloud detection or masking. As a result, cloud-contaminated pixels, cloud adjacency effects, and saturated pixels may degrade retrieval quality if not addressed upstream. Users are therefore expected to apply external cloud masks or screening procedures when high radiometric accuracy is required.

8. Error Budget and Uncertainty

8.1 Sources of Uncertainty

Uncertainty in retrieved surface reflectance arises from multiple interacting sources associated with sensor performance, atmospheric characterization, and surface properties. In ACOMP, these uncertainties propagate through both the aerosol retrieval stage and the radiative transfer inversion, ultimately affecting the accuracy of the final reflectance product. The dominant contributors include sensor calibration uncertainty, aerosol optical depth (AOD) retrieval error, atmospheric profile assumptions, and deviations from the Lambertian surface assumption Vermote, et al (2008).

Radiometric calibration uncertainty arises from residual errors in the sensor gain and offset coefficients used to convert digital numbers to top-of-atmosphere radiance. Because this

conversion is linear, calibration biases propagate directly into surface reflectance, with the largest relative impacts occurring under low signal conditions. The ACOMP processing leverages Vantor's in house capability, which is traceable to SI standards through laboratory and vicarious calibration methods and has been shown to achieve absolute radiometric agreement on the order of ~3% under well-characterized conditions, with typical operational uncertainties on the order of 3–5%[1].

Uncertainty of Aerosol optical depth (AOD) is represented using a combined absolute and relative formulation, $\Delta\tau = \pm(0.05 + 0.10\,\tau)$, where $\tau$is the retrieved AOD. This representation reflects the presence of a baseline retrieval uncertainty under low aerosol loading, together with an error component that scales with increasing aerosol concentration. When expressed as a percentage, the relative uncertainty becomes $\pm\left(\frac{0.05}{\tau} + 0.10\right) \times 100$, indicating larger fractional uncertainty in clear conditions and reduced relative uncertainty as aerosol loading increases.

AOD uncertainty is typically the dominant contributor to surface reflectance error, as it directly influences the estimation of atmospheric path radiance and both upward and downward transmittance terms in the inversion. Because ACOMP derives AOD using a scene-based retrieval approach that combines physically based modeling with heuristic constraints, uncertainties can increase in scenes lacking suitable dark or vegetated targets, or under complex atmospheric conditions such as heavy haze or strong spatial gradients. In practice, this AOD uncertainty corresponds to approximately 15–60% in relative terms and translates into surface reflectance uncertainty through its influence on atmospheric path radiance and transmittance, with the resulting reflectance error being nonlinear, spectrally dependent, and most sensitive in shorter wavelengths where aerosol scattering dominates (Vermote et al., 1997, Levy et al., 2013).

Atmospheric model and profile uncertainty, including contributions from the underlying radiative transfer modeling (e.g., MODTRAN 5.0), represents an additional source of error in surface reflectance retrieval. Uncertainty in atmospheric state parameters such as water vapor content, temperature and pressure profiles, and aerosol type can lead to inaccuracies in the estimation of atmospheric transmittance and path radiance. ACOMP relies on a combination of climatological datasets and scene-based refinement (e.g., image-derived water vapor), which may not fully capture the true atmospheric variability at the time and location of acquisition.

Radiative transfer simulations used to generate lookup tables are based on discrete atmospheric profiles and predefined aerosol models within MODTRAN 5.0 (Berk et al., 2005). While MODTRAN is a well-validated, physics-based model, it introduces approximation and discretization

[1] https://vantor.com/blog/why-you-should-care-about-absolute-radiometric-calibration

uncertainties related to spectral resolution, absorption parameterizations, and the representation of aerosol optical properties. In particular, the use of fixed aerosol models introduces structural uncertainty when actual aerosol size distributions, compositions, or vertical profiles deviate from those assumed in the simulations. These mismatches propagate through the lookup table parameterization and can affect both transmittance and path radiance terms. Quantitative evaluations of MODTRAN-based radiative transfer simulations have shown that resulting TOA radiance uncertainties can range from approximately 1–9%, depending on atmospheric conditions and input variability (Pinto et al., 2017).

Overall, atmospheric model uncertainty reflects both imperfect knowledge of the true atmospheric state and limitations in the radiative transfer representation itself and typically contributes on the order of 1–3% uncertainty in surface reflectance, depending on spectral band and atmospheric conditions.

Surface anisotropy introduces uncertainty due to the Lambertian reflectance assumption used in the inversion of 1 - 2% (Schaepman-Strub, G. et al.). Most natural surfaces exhibit bidirectional reflectance distribution function (BRDF) behavior, meaning reflectance varies with both illumination and viewing geometry. While these effects are generally modest for near-nadir observations, they can introduce systematic biases over bright, heterogeneous, or highly structured surfaces. This source of uncertainty becomes more significant for off-nadir acquisitions, where viewing geometry departs from the Lambertian assumption. Vantor satellite imagery in particular, may be collected at relatively high sensor zenith angles, and users should consider the viewing geometry when assessing product uncertainty. Additionally, Legion Mid-Inclination Orbit (MIO) sensors may acquire imagery under extreme solar illumination conditions due to flexible collection timing, further increasing sensitivity to BRDF effects and associated reflectance uncertainty.

Uncertainty in gas absorption correction arises from inaccuracies in the representation of gaseous transmittance, particularly for water vapor, ozone, and oxygen absorption features. These uncertainties are primarily driven by errors in atmospheric constituent concentrations, vertical profile assumptions, and spectroscopic parameterizations used in radiative transfer modeling. Because gas absorption is strongly wavelength-dependent, its impact on surface reflectance retrieval is highly band-specific, with the largest sensitivities occurring in absorption bands (e.g., water vapor features in the near-infrared and ozone absorption in the visible). In spectral regions with minimal gas absorption, the contribution is comparatively small. For typical atmospheric correction conditions, gas absorption uncertainty contributes approximately 0.5–2%

uncertainty in surface reflectance, depending on band placement and atmospheric variability (Vermote et al 1997, Rothman et al 2013).

Uncertainty associated with lookup table (LUT) discretization and interpolation arises from the finite sampling of the radiative transfer parameter space and the numerical methods used to approximate intermediate conditions. LUTs are generated using physics-based radiative transfer models such as MODTRAN across discrete values of key variables, including solar and viewing geometry, aerosol optical depth, and surface elevation (Berk et al., 2005). During processing, atmospheric parameters are obtained by interpolating between these discrete nodes, introducing approximation error. This error is most pronounced in regions of parameter space where radiative transfer quantities vary nonlinearly, such as under high aerosol loading or extreme viewing geometries. Such effects are inherent to LUT-based implementations of atmospheric correction models (Vermote et al., 1997) and have been shown to contribute to retrieval uncertainty when the radiative transfer space is discretized and interpolated (Verrelst et al., 2012). The magnitude of this uncertainty depends on LUT resolution and interpolation scheme but is typically on the order of 0.5–1.5% in surface reflectance. While generally smaller than aerosol or calibration uncertainties, LUT-related error represents a systematic component of the algorithm that can propagate consistently across spectral bands and scenes.

Uncertainty associated with surface elevation and the corresponding atmospheric pressure assumption arises from the use of simplified or spatially uniform elevation inputs in the radiative transfer modeling. In ACOMP, elevation is used to adjust atmospheric pressure, which in turn affects molecular (Rayleigh) scattering, gas absorption, and the overall optical path length. Because Rayleigh optical depth scales with atmospheric pressure, inaccuracies in elevation propagate into errors in scattering estimates (Bodhaine et al., 1999). When a representative or mean elevation is applied across a scene, local deviations in terrain height can introduce errors in the estimation of atmospheric transmittance and path radiance. These effects are generally modest for scenes with limited topographic variability but can become more significant in mountainous regions or areas with strong elevation gradients. The resulting impact on surface reflectance is typically on the order of 0.5–1%, with greater sensitivity observed in shorter wavelengths where Rayleigh scattering is more strongly pressure-dependent (Vermote et al. 2016).

Adjacency effects introduce uncertainty due to atmospheric scattering of radiance from neighboring pixels into the sensor line of sight (Tanré et al., 1981). This results in a mixing of radiative signals, where the observed radiance for a given pixel includes contributions not only from the target surface but also from surrounding areas. The magnitude of this effect depends on

scene heterogeneity, atmospheric conditions, and sensor spatial resolution, with stronger impacts occurring in the presence of high aerosol loading and sharp surface contrast (e.g., bright targets adjacent to dark features). Adjacency effects are particularly significant in shorter wavelengths where scattering is more pronounced. Although ACOMP accounts for adjacency contributions through parameterized correction terms within the radiative transfer framework, residual uncertainties remain due to assumptions about spatial homogeneity and the limited characterization of local radiance fields. The resulting impact on surface reflectance is typically on the order of 1–3%, but can increase in complex or highly heterogeneous scenes.

Uncertainty in extraterrestrial solar irradiance introduces a small, systematic contribution to surface reflectance error. Because solar irradiance spectra are well characterized, this effect is typically less than 1% and is spectrally smooth, making it a minor contributor relative to aerosol retrieval and radiometric calibration uncertainties.

Typical contributions from these sources, based on values reported in the literature for similar atmospheric correction frameworks, are summarized in Table 5. Aerosol retrieval uncertainty generally contributes on the order of a few percent reflectance error, while calibration and atmospheric assumptions introduce comparable but slightly smaller contributions. BRDF-related effects are typically smaller for moderate view angles but can increase under off-nadir conditions.

Table 5. Major sources of uncertainty in surface reflectance retrieval.

Error Source	Typical Contribution
Aerosol Retrieval (AOD)	2–4%
Radiometric Calibration	3–5%
Atmospheric Model / Forward model / Profile Uncertainty (including MODTRAN 5.0 radiative transfer uncertainty)	1–3%
Surface BRDF Effects (near-nadir)	1–2%
Gas Absorption Uncertainty	0.5–2% (band-dependent)
LUT Discretization / Interpolation	0.5–1.5%
Elevation / Pressure Assumption	0.5–1%
Adjacency Effects	1–3% (scene-dependent)

Error Source	Typical Contribution
Solar Irradiance	0.5–1% (systematic, spectrally dependent)

Reported uncertainty ranges represent typical magnitudes under nominal atmospheric and viewing conditions. Error sources are not strictly independent, and interactions between terms (e.g., aerosol retrieval and adjacency effects) may introduce coupled uncertainties not fully captured by individual contributions.

Actual errors are spectrally dependent and may increase in shorter wavelengths, under high aerosol loading, or in scenes with strong surface heterogeneity and adjacency effects.

8.2 Error Propagation

Uncertainty in retrieved surface reflectance arises from the combined effects of measurement error, atmospheric state uncertainty, radiative transfer modeling approximations, and algorithm assumptions. In ACOMP, these uncertainties are propagated through the atmospheric correction process using a first-order sensitivity framework that relates variability in input parameters to uncertainty in the final reflectance product.

The surface reflectance retrieval can be expressed as a function of atmospheric, geometric, and algorithm-specific variables:

$$\rho_s = f(\tau, \mathbf{p}, z, \theta_s, \theta_v, \phi, E_0, \beta, \eta_{adj}, c_{cal}) \qquad [19]$$

where these inputs represent aerosol loading, atmospheric state, surface elevation, illumination and viewing geometry, solar irradiance, surface anisotropy, adjacency effects, and sensor calibration. The propagation of uncertainty through this system is approximated using a first-order Taylor series expansion:

$$\sigma_{\rho_s}^2 = \sum_i \left(\frac{\partial \rho_s}{\partial x_i}\right)^2 \sigma_{x_i}^2 + 2 \sum_{i<j} \left(\frac{\partial \rho_s}{\partial x_i}\right)\left(\frac{\partial \rho_s}{\partial x_j}\right) \mathrm{Cov}\,(x_i, x_j) \qquad [20]$$

The first term in Equation (8-1) represents the contribution of individual (uncorrelated) uncertainties, while the second term accounts for cross-correlations between error sources. In practice, several uncertainties are not independent. Aerosol optical depth retrieval, atmospheric

model assumptions, lookup table interpolation, and adjacency effects are coupled through their shared dependence on the radiative transfer solution, and their interactions can contribute additional uncertainty beyond independent effects.

The influence of these uncertainties can be understood in the context of the radiative transfer formulation:

$$\rho_s(\lambda) = \frac{\pi\left(L_{TOA}(\lambda) - L_{path}(\lambda)\right)}{E_0(\lambda)\cos\left(\theta_s\right) T_s(\lambda)\, T_v(\lambda)} \qquad [21]$$

Radiometric calibration uncertainty affects the measured top-of-atmosphere radiance L_{TOA}, while aerosol retrieval and atmospheric model assumptions influence both path radiance L_{path} and atmospheric transmittance terms (T_s, T_v). Gas absorption introduces spectrally localized uncertainty, and LUT discretization affects all modeled quantities through interpolation. Surface anisotropy contributes model-form error due to the Lambertian assumption, and adjacency effects introduce additional path radiance from neighboring pixels. Solar irradiance contributes a small, systematic scaling uncertainty across all bands.

For clarity, the dominant contributions to reflectance uncertainty may be expressed as:

$$\sigma_{\rho_s}^2 \approx \left(\frac{\partial \rho_s}{\partial \tau}\sigma_\tau\right)^2 + \left(\frac{\partial \rho_s}{\partial c_{cal}}\sigma_{cal}\right)^2 + \left(\frac{\partial \rho_s}{\partial m_{atm}}\sigma_m\right)^2 + \left(\frac{\partial \rho_s}{\partial \beta}\sigma_\beta\right)^2 + \left(\frac{\partial \rho_s}{\partial g}\sigma_g\right)^2 + \left(\frac{\partial \rho_s}{\partial \delta_{LUT}}\sigma_{LUT}\right)^2$$
$$+ \left(\frac{\partial \rho_s}{\partial z}\sigma_z\right)^2 + \left(\frac{\partial \rho_s}{\partial \eta_{adj}}\sigma_{adj}\right)^2 + \left(\frac{\partial \rho_s}{\partial E_0}\sigma_{E_0}\right)^2 \qquad [22]$$

where each term corresponds to a specific uncertainty source identified in Section 8.1.

In operational implementation, the full covariance structure in Equation (8-1) is not explicitly evaluated due to computational constraints and limited knowledge of parameter correlations. Instead, ACOMP estimates uncertainty using band-specific sensitivity analysis, in which key parameters are perturbed within their expected uncertainty ranges and the resulting change in surface reflectance is computed numerically:

$$\delta\rho_s(\lambda) \approx \sum_i \left| \frac{\partial \rho_s(\lambda)}{\partial x_i} \right| \delta x_i \qquad [23]$$

This approach captures both direct parameter effects and nonlinear behavior introduced by radiative transfer modeling and LUT interpolation. The resulting uncertainty is strongly wavelength dependent, with aerosol-related effects dominating in shorter wavelengths due to enhanced scattering, while calibration and transmittance-related uncertainties become relatively more important at longer wavelengths.

The uncertainty sources described in Section 8.1 propagate through the radiative transfer inversion via their influence on path radiance and atmospheric transmittance. Radiometric calibration primarily affects L_{TOA}, aerosol retrieval affects both $L_{path}$and $(T_s{}', T_v)$, and atmospheric profile assumptions influence transmittance estimates. LUT interpolation introduces systematic approximation error, while surface anisotropy and adjacency effects contribute scene-dependent bias. The relative importance of each contribution is spectrally dependent and is quantified through the sensitivity analysis described above.

For completeness, the primary variables used in this formulation are defined as follows. Surface reflectance is denoted by ρ_s, with associated uncertainty σ_{ρ_s}. Aerosol optical depth is τ with uncertainty σ_τ. Radiometric calibration parameters are represented by c_{cal} with uncertainty σ_{cal}. Atmospheric model parameters, including water vapor and pressure, are denoted m_{atm} with uncertainty σ_m. Surface anisotropy is represented by β with uncertainty σ_β, and gas absorption parameters by g with uncertainty σ_g. LUT interpolation effects are denoted δ_{LUT} with uncertainty σ_{LUT}, and surface elevation is z with uncertainty σ_z. Adjacency radiance contribution is η_{adj} with uncertainty σ_{adj}, and extraterrestrial solar irradiance is E_0 with uncertainty σ_{E_0}. Solar zenith angle, sensor zenith angle, and relative azimuth are given by θ_s, θ_v, and ϕ, respectively.

Table 6 summarizes the relationship between the uncertainty sources described above, the radiative transfer variables they influence, and their spectral sensitivity characteristics. Overall, this framework provides a physically consistent and computationally practical representation of uncertainty propagation within the ACOMP atmospheric correction algorithm, with dominant contributions typically arising from aerosol retrieval and radiometric calibration, particularly in shorter wavelengths.

Table 6. Mapping Uncertainty Sources to Radiative Transfer Terms and Spectral Sensitivity

Error Source	Affected Radiative Transfer Variables	Spectral Sensitivity Characteristics
Radiometric Calibration (c_{cal})	$L_{TOA}(\lambda)$	Broad impact across all bands; propagates linearly into reflectance; larger relative impact in low-signal conditions

Error Source	Affected Radiative Transfer Variables	Spectral Sensitivity Characteristics
Aerosol Retrieval (AOD, τ)	$L_{path}(\lambda), T_s(\lambda), T_v(\lambda)$	Strongest in blue and visible wavelengths due to scattering; decreases toward NIR
Atmospheric Model / Profile (m_{atm})	$T_s(\lambda), T_v(\lambda)$	Band-dependent; driven by water vapor, pressure, and temperature profile variability
Gas Absorption (g)	$T_s(\lambda), T_v(\lambda)$	Localized to absorption features (e.g., H_2O, O_3); minimal impact outside absorption bands
Surface Anisotropy (BRDF, β)	$\rho_s(\lambda)$(model assumption)	Increases with off-nadir viewing and large solar zenith angles; scene-dependent
LUT Discretization / Interpolation (δ_{LUT})	$L_{path}(\lambda), T_s(\lambda), T_v(\lambda)$	Smooth, systematic effect; depends on LUT resolution and parameter spacing
Elevation / Pressure (z)	$L_{path}(\lambda), T_s(\lambda), T_v(\lambda)$	Moderate impact; more pronounced in shorter wavelengths due to Rayleigh scattering dependence on pressure
Adjacency Effects (η_{adj})	Effective $L_{path}(\lambda)$	Strongest in high-scatter bands (blue/green); increases with scene heterogeneity and aerosol loading
Solar Irradiance (E_0)	$E_0(\lambda)$	Small, systematic, spectrally smooth scaling effect across all bands

Values in Table 7 represent illustrative, band-dependent uncertainty contributions based on typical ACOMP sensitivity behavior and expected parameter variability. The combined uncertainty is estimated using a root-sum-square (RSS) approach assuming independent error sources; covariance terms described in Equation 20 are not explicitly included. Actual uncertainty may vary depending on scene conditions, atmospheric state, viewing geometry, and surface characteristics. Uncertainty is generally higher in shorter wavelengths due to increased sensitivity to aerosol scattering and adjacency effects, and lower in longer wavelengths where these effects are reduced.

The propagated uncertainty estimates presented here provide an expected error range under nominal conditions. Actual product accuracy, as evaluated through validation against reference measurements, is discussed in Section 8.3.

Table 7. Example Band-Dependent Surface Reflectance Uncertainty (Illustrative)

Error Source	Blue	Green	Red	NIR
Aerosol Retrieval (AOD, τ)	3.5%	2.5%	1.8%	1.0%
Radiometric Calibration (c_{cal})	3.0%	3.0%	3.0%	3.0%
Atmospheric Model / Profile (m_{atm})	2.0%	2.0%	2.0%	1.5%
Surface Anisotropy (BRDF, β)	1.0%	1.0%	1.2%	1.5%
Gas Absorption (g)	0.8%	0.5%	0.7%	1.5%
LUT Discretization / Interpolation (δ_{LUT})	1.0%	1.0%	1.0%	1.0%
Elevation / Pressure (z)	0.8%	0.6%	0.5%	0.3%
Adjacency Effects (η_{adj})	2.5%	1.5%	1.0%	0.5%
Solar Irradiance (E_0)	0.5%	0.5%	0.5%	0.5%
Combined Uncertainty (RSS)	**5.9%**	**4.9%**	**4.4%**	**4.2%**

The band-dependent uncertainty values in Table 7 are derived from representative midpoint values of the uncertainty ranges summarized in Table 5, with adjustments applied based on the known spectral sensitivity of each error source. Aerosol retrieval and adjacency effects are emphasized in shorter wavelengths due to increased scattering, while their influence decreases toward the near infrared. Gas absorption uncertainty is enhanced in bands affected by absorption features, particularly in the NIR. Elevation and pressure-related effects are more significant at shorter wavelengths due to Rayleigh scattering dependence. Radiometric calibration and LUT interpolation are treated as spectrally uniform, while BRDF-related uncertainty increases modestly in longer wavelengths and off-nadir viewing conditions. These values represent physically informed approximations rather than direct outputs of the operational algorithm and are consistent with the band-specific sensitivity behavior described in Equation (8-3), where parameter perturbations produce wavelength-dependent responses in retrieved surface reflectance.

8.3 Expected Accuracy

The expected accuracy of the ACOMP surface reflectance product is informed by both the uncertainty propagation analysis described in Section 8.2 and comparisons to established atmospheric correction performance benchmarks. Under nominal atmospheric conditions and for well-calibrated imagery, surface reflectance retrieval accuracy is expected to be on the order of approximately 4–6% reflectance, depending on spectral band and scene characteristics.

Accuracy is inherently wavelength dependent. Shorter wavelengths (e.g., blue and green bands) generally exhibit larger errors due to increased sensitivity to aerosol scattering and adjacency effects, while longer wavelengths (e.g., red and near-infrared) typically achieve improved accuracy due to reduced atmospheric scattering and more stable transmittance behavior. These trends are consistent with the band-dependent uncertainty estimates presented in Table 7.

The dominant contributors to reflectance error are aerosol optical depth (AOD) retrieval and radiometric calibration. Aerosol-related uncertainty has the largest impact in shorter wavelengths, where small errors in AOD propagate strongly into path radiance and transmittance terms. Radiometric calibration introduces a spectrally consistent uncertainty across all bands and establishes a baseline accuracy limit. Additional contributions arise from atmospheric model assumptions, gas absorption, lookup table interpolation, surface anisotropy, and adjacency effects, each of which contributes in a band- and scene-dependent manner.

It is important to note that the reported accuracy represents expected performance under typical conditions and does not account for all possible sources of scene-specific variability. Accuracy may degrade in cases of heavy aerosol loading, complex or rapidly varying atmospheric conditions, high sensor or solar zenith angles, or highly heterogeneous surfaces where adjacency and BRDF effects are more pronounced. Conversely, improved accuracy may be achieved under clear atmospheric conditions with well-constrained aerosol retrieval and near-nadir viewing geometry.

The expected accuracy described here is consistent with the propagated uncertainty estimates derived from the algorithm formulation and reflects the combined influence of measurement, modeling, and environmental factors. Validation against independent reference datasets (e.g., ground-based measurements or cross-sensor comparisons) is used to further assess and refine these accuracy estimates, as described in Section 9.

9. Validation Results

Validation of the ACOMP surface reflectance product is performed through comparison with independent ground-based measurements, atmospheric observations, and cross-method analysis. These activities provide an empirical assessment of algorithm performance and support the expected accuracy described in Section 8.

The validation dataset includes over 5,000 ASD field measurements collected across six geographically and climatically diverse locations, as well as approximately 1,000 WorldView-2 images acquired between 2010 and 2014. Measurements were collected over stable, well-characterized targets (e.g., asphalt, concrete) with BRDF sampling to account for directional reflectance effects.

Comparison of ACOMP-derived surface reflectance with ASD measurements indicates strong agreement across all spectral bands. As shown in Figure 5, retrieved reflectance values are closely aligned with field observations, with regression slopes near unity (approximately 1.0–1.04) and minimal intercept bias. The observed scatter about the 1:1 line corresponds to reflectance differences typically on the order of 4–6% under nominal conditions, consistent with the propagated uncertainty estimates presented in Section 8.

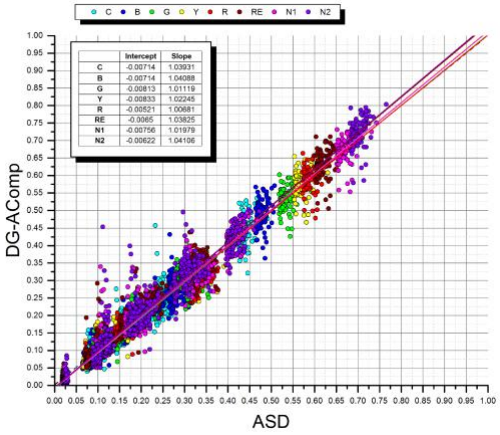

Figure 5. Surface Reflectance Comparison to ASD.

Atmospheric consistency is evaluated through comparison of retrieved AOD with AERONET and MODIS observations. As shown in Figure 9-2, ACOMP AOD retrievals exhibit slopes generally near unity relative to reference datasets, indicating physically consistent atmospheric characterization. Some variability is observed due to spatial mismatch between satellite imagery and ground-based measurements, as well as differences in temporal sampling.

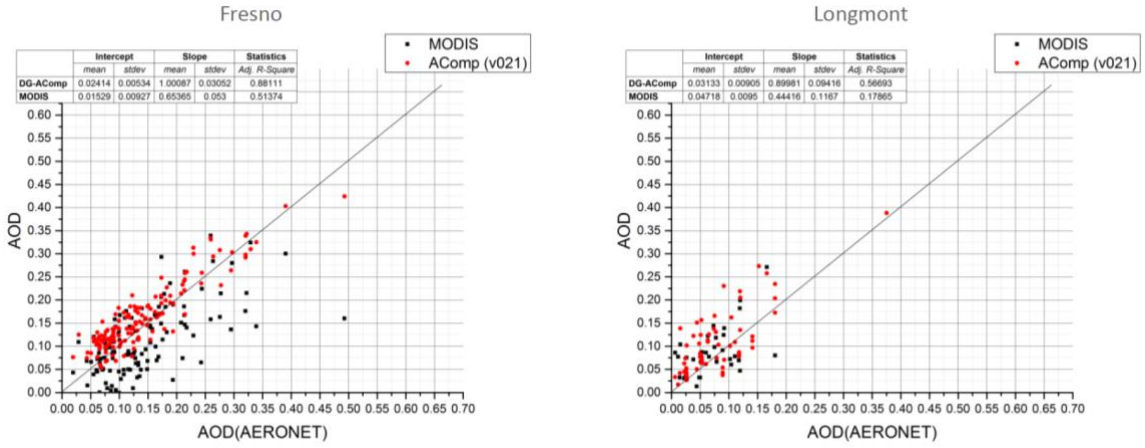

Figure 6. AOD Comparison to AERONET and MODIS over sites in Fresno, AZ and Longmont, CO.

Algorithm performance is further evaluated through comparison with established atmospheric correction methods. As shown in Figure 7, ACOMP demonstrates lower RMSE relative to QUAC and comparable or improved performance relative to FLAASH across spectral bands. These results are consistent with the expected behavior of a physically based, scene-adaptive atmospheric correction approach.

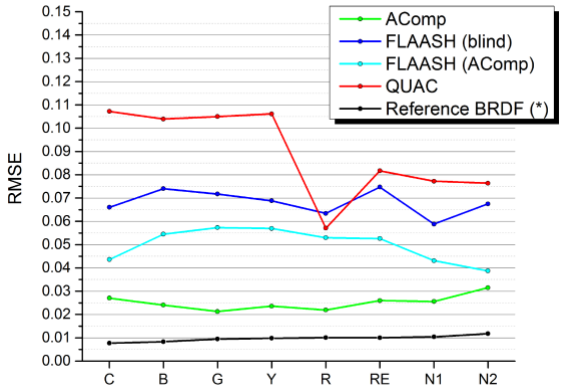

Figure 7. RMSE Comparison to FLAASH and QUAC.

Temporal consistency of the ACOMP surface reflectance product is illustrated in Figure 8. Variability in the original imagery due to changing atmospheric conditions, including haze and scattering effects, is reduced after correction, resulting in improved consistency of surface reflectance across acquisition dates. This effect is particularly evident in regions affected by variable haze conditions and is consistent with the removal of path radiance and atmospheric transmittance effects described in Section 5.

Figure 8. Multi-temporal comparison of original imagery (top row) and ACOMP surface reflectance (bottom row) over Hanoi, Vietnam.

In Figure 8, the original imagery exhibits significant variability in atmospheric conditions, including haze and scattering effects, which introduce changes in apparent surface brightness and color across acquisition dates. After atmospheric correction, the ACOMP surface reflectance product shows improved temporal consistency, with reduced atmospheric influence and more stable spectral response across time.

Overall, validation results indicate that ACOMP surface reflectance achieves agreement with independent reference measurements typically within 4–6% reflectance under nominal atmospheric and viewing conditions. Accuracy degrades in the presence of high aerosol loading, complex atmospheric structure, or extreme viewing geometry, consistent with the uncertainty characterization described in Section 8.

10. Known Limitations

The ACOMP algorithm performs robust atmospheric correction under a wide range of conditions; however, several known limitations remain. Retrieval accuracy can degrade over very bright surfaces, where high reflectance reduces the contrast needed for reliable aerosol estimation and

increases sensitivity to model assumptions. Similarly, scenes with heavy aerosol loading present challenges, as the inversion becomes less stable at high optical depths and may lead to over- or under-correction depending on the available constraints.

Cloud-related effects also introduce uncertainty. Adjacency effects near clouds can contaminate neighboring pixels, leading to biased reflectance estimates even when clouds themselves are masked. Translucent cirrus clouds are particularly problematic, as they may not be fully detected yet still contribute additional scattering, resulting in residual atmospheric artifacts. More generally, spatially variable haze can be difficult to fully characterize, especially when its distribution is not well captured by the AOD retrieval approach.

The algorithm relies on internally derived atmospheric parameters, including aerosol optical depth and water vapor, which are estimated directly from the image and ancillary climatology rather than in-situ measurements. As a result, retrieval accuracy is dependent on scene content and may be limited in cases where suitable dark or vegetated targets are not present. In addition, the algorithm currently uses a fixed solar irradiance reference spectrum, and any inconsistencies or updates to that reference (e.g., choice of solar model) may introduce small systematic biases.

These limitations should be considered when interpreting results, particularly in scenes with extreme atmospheric conditions, complex cloud structures, or limited surface diversity.

11. Future Improvements

Future development of ACOMP will focus on improving accuracy, robustness, and adaptability across diverse atmospheric and surface conditions.

Key enhancements include refinement of aerosol modeling through incorporation of more advanced and regionally adaptive aerosol representations, improving performance in complex and high-loading atmospheric conditions. Continued evolution of radiative transfer lookup tables (LUTs) is also planned, including updates to newer radiative transfer model versions and increased parameter resolution to reduce interpolation error.

Additional improvements include incorporation of spatially varying elevation to better represent terrain-driven atmospheric variability, as well as enhanced treatment of adjacency effects through more advanced spatial modeling approaches. Refinement of water vapor estimation and gas absorption parameterization will further improve spectral accuracy.

Future implementations may also integrate external atmospheric data sources, such as numerical weather models or reanalysis datasets, to better constrain atmospheric state under challenging conditions. Advances in computational capability may enable direct radiative transfer

simulations or hybrid LUT–model approaches, reducing reliance on precomputed lookup tables and improving physical fidelity.

12. Product Usage Guidance

ACOMP surface reflectance products are distributed as scaled integer values within GeoTIFF files. The pixel values represent surface reflectance scaled by a factor determined by the data delivery pathway. To convert pixel values to unitless surface reflectance (typically ranging from 0 to 1), users must apply the appropriate scaling factor.

For imagery delivered through standard Vantor processing (native sensor scaling), the scaling factor is determined by the sensor bit depth:

$$\rho = \frac{DN}{2^b - 1} \quad [24]$$

where ρ is surface reflectance, DN is the pixel value, and b is the sensor bit depth.

For example, for a WorldView Legion image (14-bit), the maximum DN is $2^{14} - 1 = 16383$. A pixel value of 2050 corresponds to a surface reflectance of:

$$\rho = \frac{2050}{16383} \approx 0.125 \quad [25]$$

For imagery distributed through the Vantor HUB or NASA CDSA project (fixed scaling), surface reflectance values are scaled to a range of 0–10,000. In this case, the conversion is:

$$\rho = \frac{DN}{10000} \quad [26]$$

Users should confirm the data delivery pathway for all of their ACOMP imagery to determine the appropriate scaling method. Scaling does not affect relative reflectance values within an image but must be applied correctly to obtain physically meaningful reflectance values for quantitative analysis. This scaling approach is consistent with the output surface reflectance representation described in Section 5.11.

Table 8. Sensor Bit Depth and Scaling Factors

Sensor	Spectral Range	Bit Depth (b)	Max DN (2^b – 1)	Native Sensor Scaling (Standard Delivery)	Fixed Scaling (Vantor HUB)
WorldView-1 (WV01)	PAN	11	2047	DN / 2047	DN / 10000
GeoEye-1 (GE01)	VNIR	11	2047	DN / 2047	DN / 10000

Sensor	Spectral Range	Bit Depth (b)	Max DN (2^b – 1)	Native Sensor Scaling (Standard Delivery)	Fixed Scaling (Vantor HUB)
WorldView-2 (WV02)	VNIR	11	2047	DN / 2047	DN / 10000
WorldView-3 (WV03)	VNIR	11	2047	DN / 2047	DN / 10000
WorldView-3 (WV03)	SWIR	14	16383	DN / 16383	DN / 10000
WorldView Legion (LG01 – LG06)	VNIR	14	16383	DN / 16383	DN / 10000

13. Summary

The ACOMP algorithm provides a radiative transfer–based approach for converting top-of-atmosphere (TOA) radiance into surface reflectance by accounting for atmospheric scattering, absorption, and adjacency effects. The algorithm combines precomputed lookup tables (LUTs) derived from radiative transfer simulations with scene-based estimation of atmospheric parameters, including aerosol optical depth (AOD) and water vapor, to enable efficient and physically consistent atmospheric correction across a range of sensors and imaging conditions.

Through its hybrid design, which integrates radiative transfer modeling, LUT interpolation, and spatially adaptive parameter estimation, ACOMP achieves a balance between physical consistency and computational efficiency. Surface reflectance is retrieved on a per-pixel basis while maintaining a stable atmospheric solution, enabling consistent quantitative analysis across time, geographic regions, and sensor platforms. Uncertainty characterization and validation results demonstrate that the algorithm provides reliable performance under nominal conditions, with known limitations in scenes exhibiting strong spatial heterogeneity, high aerosol loading, or complex atmospheric structure.

Future enhancements will focus on improving the representation of atmospheric variability and advancing the underlying radiative transfer framework. Planned developments include refinement of aerosol modeling, updates to radiative transfer LUTs using improved spectroscopic data and modeling capabilities, and incorporation of spatially varying elevation and atmospheric parameters. Additional work will explore enhanced treatment of adjacency effects, improved water vapor characterization, and integration of external atmospheric datasets. Advances in computational capability may also enable hybrid or direct radiative transfer approaches, reducing reliance on precomputed LUTs while maintaining operational efficiency.

14. References

Basith, A., & Prastyani, R. (2020). Evaluating ACOMP, FLAASH and QUAC on Worldview-3 for satellite derived bathymetry (SDB) in shallow water. *Geodesy and Cartography*, *46*(3), 151-158. https://doi.org/10.3846/gac.2020.11426

Berk, A., Anderson, G. P., Acharya, P. K., Bernstein, L. S., Muratov, L., Lee, J., Fox, M. J., Adler-Golden, S. M., Chetwynd, J. H., Hoke, M. L., Lockwood, R. B., Gardner, J. A., Cooley, T. W., Borel, C. C., & Lewis, P. E. (2005). MODTRAN 5: A reformulated atmospheric band model with auxiliary species and practical multiple scattering options. Proceedings of SPIE, 5806, Algorithms and Technologies for Multispectral, Hyperspectral, and Ultraspectral Imagery XI. https://doi.org/10.1117/12.606026

Bodhaine, B. A., Wood, N. B., Dutton, E. G., & Slusser, J. R. (1999). On Rayleigh optical depth calculations. Journal of Atmospheric and Oceanic Technology, 16(11), 1854–1861. https://doi.org/10.1175/1520-0426(1999)016<1854:ORODC>2.0.CO;2

Levy, R. C., Mattoo, S., Munchak, L. A., Remer, L. A., Sayer, A. M., Patadia, F., & Hsu, N. C. (2013). The Collection 6 MODIS aerosol products over land and ocean. Atmospheric Measurement Techniques, 6, 2989–3034. https://doi.org/10.5194/amt-6-2989-2013

Ochoa, T. (2026). *Absolute radiometric calibration sensitivity analysis of Vantor's surface reflectance product* [Master's thesis, University of Arizona]. UA Campus Repository. http://hdl.handle.net/10150/679931

Pacifici, F. (2012). An automatic atmospheric compensation algorithm for very high spatial resolution imagery. *Society of Photo-optical Instrumentation Engineers Defense, Security, and Sensing (SPIE)*.

Pacifici, F., Longbotham, N., Lester, D., Bader, B., Balasalle, J., Karspeck, M., Kuester, M., & Miecznik, G. (2014). Validation of the DigitalGlobe surface reflectance product and its comparison to FLAASH and QUAC. (2015). The Joint Agency Commercial Imagery Evaluation (JACIE), Reston, VA.

Pacifici, F. (2016, July). Validation of the DigitalGlobe surface reflectance product. In *2016 IEEE International Geoscience and Remote Sensing Symposium (IGARSS)* (pp. 1973-1975). IEEE.

Pinto, C. T., Castro, R. M., Ponzoni, F. J., Leigh, L., & Helder, D. (2017). Uncertainty evaluation of the TOA radiance predicted by MODTRAN-5. Proceedings of the XVIII Brazilian Symposium on Remote Sensing (SBSR), INPE, Santos, Brazil.

Rothman, L. S., Gordon, I. E., Babikov, Y., Barbe, A., Benner, D. C., Bernath, P. F., Birk, M., Bizzocchi, L., Boudon, V., Brown, L. R., Campargue, A., Chance, K., Cohen, E. A., Coudert, L. H., Devi, V. M., Drouin, B. J., Fayt, A., Flaud, J.-M., Gamache, R. R., ... Wagner, G. (2013). The HITRAN2012 molecular spectroscopic database. Journal of Quantitative Spectroscopy and Radiative Transfer, 130, 4–50. https://doi.org/10.1016/j.jqsrt.2013.07.002

Schaepman-Strub, G., Schaepman, M. E., Painter, T. H., Dangel, S., & Martonchik, J. V. (2006). Reflectance quantities in optical remote sensing—Definitions and case studies. Remote Sensing of Environment, 103(1), 27–42. https://doi.org/10.1016/j.rse.2006.03.002

Tanré, D., Herman, M., & Deschamps, P. Y. (1981). Influence of the background contribution upon space measurements of ground reflectance. Applied Optics, 20(20), 3676–3684. https://doi.org/10.1364/AO.20.003676

U.S. Patent US20190130547A1. (2019). Atmospheric compensation in satellite imagery.

Verrelst, J., Muñoz, J., Alonso, L., Delegido, J., Rivera, J. P., Camps-Valls, G., & Moreno, J. (2012). Machine learning regression algorithms for biophysical parameter retrieval: Opportunities for Sentinel-2 and -3. Remote Sensing of Environment, 118, 127–139. https://doi.org/10.1016/j.rse.2011.11.002

Vermote, E. F., Tanré, D., Deuzé, J. L., Herman, M., & Morcette, J. J. (1997). Second simulation of the satellite signal in the solar spectrum, 6S: An overview. IEEE Transactions on Geoscience and Remote Sensing, 35(3), 675–686. https://doi.org/10.1109/36.581987

Vermote, E. F., & Kotchenova, S. Y. (2008). Atmospheric correction for the monitoring of land surfaces. Journal of Geophysical Research: Atmospheres, 113(D23). https://doi.org/10.1029/2007JD009662

Vermote, E. F., Justice, C. O., Claverie, M., & Franch, B. (2016). Preliminary analysis of the performance of the Landsat 8/OLI land surface reflectance product. Remote Sensing of Environment, 185, 46–56. https://doi.org/10.1016/j.rse.2016.04.008